

Research



Cite this article: Li J, Fei Z-y, Xu Y-f, Wang J, Fan B-f, Ma X-j, Wang G. 2018 Study on the optimization of the deposition rate of planetary GaN-MOCVD films based on CFD simulation and the corresponding surface model. *R. Soc. open sci.* **5**: 171757.
<http://dx.doi.org/10.1098/rsos.171757>

Received: 2 November 2017

Accepted: 10 January 2018

Subject Category:

Engineering

Subject Areas:

vacuum physics/fluid mechanics/
chemical engineering

Keywords:

gallium nitride, metal-organic chemical vapour deposition, numerical simulation, epitaxial growth, deposition rate, response surface methodology method

Author for correspondence:

Gang Wang

e-mail: stswangg@mail.sysu.edu.cn


Study on the optimization of the deposition rate of planetary GaN-MOCVD films based on CFD simulation and the corresponding surface model

Jian Li¹, Ze-yuan Fei¹, Yi-feng Xu¹, Jie Wang¹,
Bing-feng Fan², Xue-jin Ma¹ and Gang Wang^{1,3}

¹School of Electronics and Information Technology, Sun Yat-sen University, Guangzhou 51000, People's Republic of China

²Institute of Advanced Technology, Sun Yat-sen University, Guangzhou 510275, People's Republic of China

³State Key Laboratory of Optoelectronic Materials and Technologies, Guangzhou 510275, People's Republic of China

 JL, 0000-0002-6033-2141

Metal-organic chemical vapour deposition (MOCVD) is a key technique for fabricating GaN thin film structures for light-emitting and semiconductor laser diodes. Film uniformity is an important index to measure equipment performance and chip processes. This paper introduces a method to improve the quality of thin films by optimizing the rotation speed of different substrates of a model consisting of a planetary with seven 6-inch wafers for the planetary GaN-MOCVD. A numerical solution to the transient state at low pressure is obtained using computational fluid dynamics. To evaluate the role of the different zone speeds on the growth uniformity, single factor analysis is introduced. The results show that the growth rate and uniformity are strongly related to the rotational speed. Next, a response surface model was constructed by using the variables and the corresponding simulation results. The optimized combination of the matching of different speeds is also proposed as a useful reference for applications in industry, obtained by a response surface model and genetic algorithm with a balance between the growth rate and the growth uniformity. This method can save time, and the optimization can obtain the most uniform and highest thin film quality.

1. Introduction

GaN-based III-V compound semiconductor thin films are important third-generation semiconductor materials, which are widely used in the manufacture of blue-violet light-emitting diodes, semiconductor lasers and high-frequency, high-power electronic equipment [1–6]. Metal-organic chemical vapour deposition (MOCVD) is an important technology for growing GaN thin films due to its advantages such as the large epitaxy area, good reproducibility and high deposition rate [7–11].

Film thickness uniformity is an important index to measure the quality of film growth. In general, the more uniform the film thickness, the more uniform the distribution of components, and the higher the quality of the thin film. The quality of thin film is related to many parameters, such as the gas inlet flow rate, reactor pressure, rotation speed of the base and temperature of the substrate. In order to obtain uniform composition and film thickness, gas flows are required to be laminar. In such a laminar flow, vortices do not occur near the substrate, the gas flow in the direction parallel to the substrate has a uniform temperature field in the direction vertical to the substrate with a high temperature difference, and the particle concentration near the substrate should be as uniform as possible [12–16]. In general, coefficient variation of less than 5% is considered to be important for usable thin films. However, owing to the actual flow state in the reaction chamber, the temperature field and chemical composition of the reaction chamber cannot be visualized by the equipment operator, which introduces unknowns in the process of growth and adjustment.

Fortunately, computational fluid dynamics (CFD) is highly useful for the development of MOCVD equipment. Dimitrios *et al.*, in an early study of the cavity flow state [17–19], investigated the particle flow of TiO in a vertical spray reaction chamber, and using the fluid model calculation results and particles in the reaction chamber of the control flow graph experiment, obtained the flow state to determine the feasibility of the numerical simulation. In addition, Theodoropoulos and others investigated the chemical mechanism model [20,21] to study the reaction chamber and coupled field, and proposed a model for the influence of different process parameters on the deposition rate under different conditions. With the improvement of GaN-MOCVD growth mechanism models, scholars such as Mitrovic studied the influence of different process parameters on deposition rate and optimized the design of reaction chambers [22–31].

At present, the planetary MOCVD chamber can adequately solve the problem relating to the thickness uniformity of large volume and large capacity film deposition. Planetary MOCVD is conducive to large size, large modulus and production of thin films, because it can be operated at low rotational speeds; this avoids large centrifugal forces that lead to film delamination. However, there is little research on the influence of the coupling between different rotation speeds on the flow rate and deposition rate. However, a few research groups have theoretically studied the method to adjust the speed of the different regions to find the optimum deposition rate. It is a difficult problem to adjust the uniformity of the film because of the complex coupling field. The simplest method is to adjust film deposition rate by rotating speed.

This study uses the rotation speeds of the substrate and wafers as variable parameters, and other conditions remain unchanged. The quality of MOCVD films was simulated and optimized, and the variation coefficient of thin film thicknesses was used as a measure of the uniformity and the quality of thin film growth. We present the rotation speeds of substrate and wafers as the input variables, the deposition rates as outputs, and the variation coefficient of the deposition rates are used as a response. First, 100 sets of input and output values are obtained by the design of experiment (DOE) method, and then the response surface model is constructed; finally, optimal results are obtained by using a response surface model (RSM) and a genetic algorithm.

2. Mathematical formulation

2.1. Governing equations

GaN film growth occurs in a state of low pressure, laminar flow and steady state during the growth of MOCVD. Its mathematical model includes the conservation of mass, momentum, energy and individual species.

The conservation equations and conservation equation of momentum are provided [32–34]:

$$\nabla \cdot (\rho \mathbf{v}) = 0 \quad (2.1)$$

Table 1. Gas-phase kinetic scheme for MOCVD of GaN from TMG and ammonia. k_0 : activation energy (kcal/mol), E : pre-exponential factor (1/s), β : temperature influence factor.

reactions	k_0	E	β
(G1) $\text{Ga}(\text{CH}_3)_3 \rightarrow \text{Ga}(\text{CH}_3)_2 + \text{CH}_3$	3.5×10^{15}	59.5	0
(G2) $\text{Ga}(\text{CH}_3)_2 \rightarrow \text{GaCH}_3 + \text{CH}_3$	8.7×10^7	35.4	0
(G3) $\text{Ga}(\text{CH}_3)_3 + \text{NH}_3 \rightarrow (\text{CH}_3)_3\text{Ga} : \text{NH}_3$	1×10^{12}	0	0
(G4) $(\text{CH}_3)_3\text{Ga} : \text{NH}_3 \rightarrow \text{Ga}(\text{CH}_3)_3 + \text{NH}_3$	1×10^{14}	18.5	0
(G5) $(\text{CH}_3)_3\text{Ga} : \text{NH}_3 \rightarrow (\text{CH}_3)_2\text{Ga} : \text{NH}_2 + \text{CH}_4$	1×10^{14}	49	0

and

$$\nabla \cdot (\rho \mathbf{v} \cdot \mathbf{v}) = \nabla \bar{\tau} - \nabla p + \rho \mathbf{g}, \quad (2.2)$$

where ρ and \mathbf{v} are the density and velocity vectors of the gas mixture, respectively, and p and \mathbf{g} are the pressure and gravitational acceleration, respectively. $\bar{\tau}$ is the shear stress tensor expressed by

$$\bar{\tau} = \mu(\nabla \mathbf{v} + (\nabla \mathbf{v})^T) - \frac{2}{3}\mu(\nabla \cdot \mathbf{v}) \cdot \mathbf{I}, \quad (2.3)$$

where μ is the viscosity, and \mathbf{I} is the unit tensor.

The energy equation is given by

$$C_p \nabla \cdot (\rho \mathbf{v} T) = \nabla \cdot (k \nabla T) + \sum_{i=1}^N \frac{H_i}{M_i} \nabla \cdot \mathbf{J}_i - \sum_{i=1}^N \frac{H_{i,0}}{M_i} R_i, \quad (2.4)$$

where C_p is the specific heat capacity at a constant pressure, k is the thermal conductivity and T is the temperature. In addition, H_i , $H_{i,0}$, M_i and \mathbf{J}_i represent the molar enthalpy, enthalpy of formation, molar mass and diffusion flux of the species, respectively.

We employ a finite rate translation model to simulate the growth of GaN, which can be described by

$$\nabla \cdot (\rho \mathbf{v} w_i) = -\nabla \cdot \mathbf{J}_i + M_i \sum_{j=1}^K R_j^i, \quad (2.5)$$

where w_i is the mass fraction of species i and R_j^i is the net volumetric rate of creation of species i during reaction j .

The density of the gas mixture is defined by

$$\rho = \frac{P_{\text{op}} M_w}{RT}, \quad (2.6)$$

where P_{op} , M_w and R are the operating pressure, molecular weight of the gas and universal gas constant, respectively.

2.2. Reaction mechanisms

At present, the typical GaN-MOCVD is carried by the carrier gas ammonia (NH_3), carrying the metal-organic source precursor $\text{Ga}(\text{CH}_3)_3$ (TMG) and nitride through the top of the uniquely designed spray mixing device into the reaction chamber. From detailed studies by other researchers, it is known that the complex gas will undergo complex gas and surface chemical reactions in the MOCVD reaction chamber and produce a large number of intermediate products. This paper uses the existing GaN growth reaction mechanism, including five gas-phase reactions and five surface reactions to simulate the growth [20,21,31,35], as shown in tables 1 and 2, respectively.

To evaluate the uniformity of film thickness, the coefficient of variation is introduced. It is an absolute value reflecting the degree of data dispersion, and measures the degree of variation of the observed data.

$$\bar{x} = \frac{\sum_{i=1}^n x_i \times S_i}{S} \quad (2.7)$$

$$C = \frac{\sqrt{1/n - 1 \sum_{i=1}^n (x_i - \bar{x})^2}}{\bar{x}}, \quad (2.8)$$

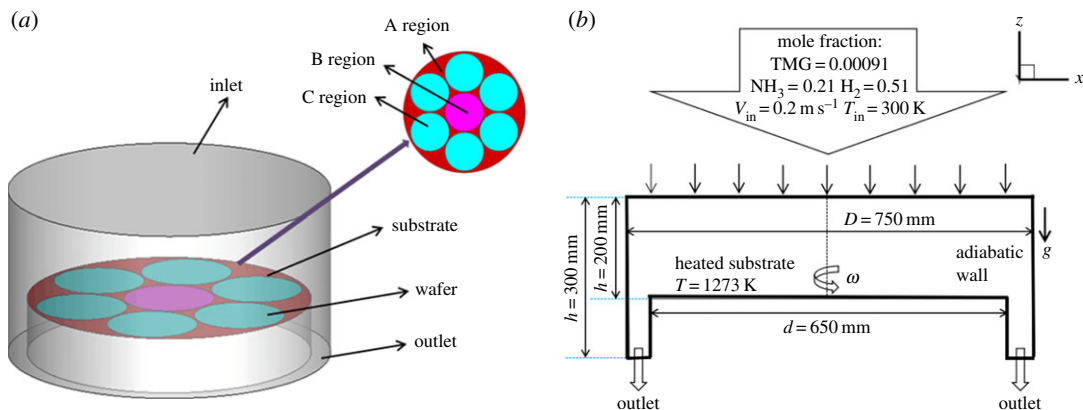


Figure 1. (a) GaN-MOCVD Reactor model. (b) Gas flow diagram of GaN-MOCVD.

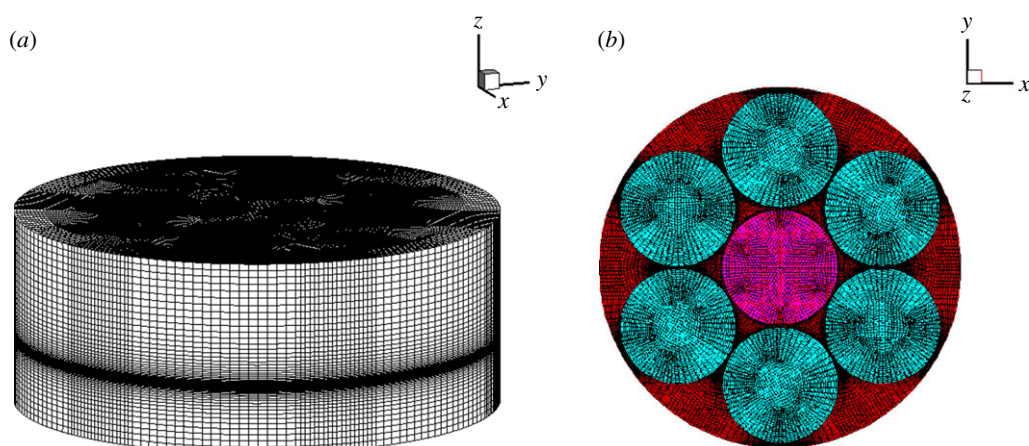


Figure 2. (a) The complete mesh of the GaN-MOCVD reactor. (b) Substrate grid diagram of GaN-MOCVD reactor.

Table 2. Gas–surface interactions in metal-organic vapour phase epitaxy (MOVPE) of GaN. S denotes a free surface site and $s = 1$ denotes a unity sticking coefficient at zero coverage.

reactions	k_0	E
(S1) $\text{Ga}(\text{CH}_3)_3 + \text{S} \rightarrow \text{Ga}(\text{B}) + 3\text{CH}_3$	$s = 1$	0
(S2) $\text{Ga}(\text{CH}_3)_2 + \text{S} \rightarrow \text{Ga}(\text{B}) + 2\text{CH}_3$	$s = 1$	0
(S3) $\text{GaCH}_3 + \text{S} \rightarrow \text{Ga}(\text{B}) + \text{CH}_3$	$s = 1$	0
(S4) $(\text{CH}_3)_3\text{Ga} : \text{NH}_3 + 2\text{S} \rightarrow \text{GaN}(\text{B}) + 3\text{CH}_4$	$s = 1$	0
(S5) $(\text{CH}_3)_2\text{Ga} : \text{NH}_2 + 2\text{S} \rightarrow \text{GaN}(\text{B}) + 2\text{CH}_4$	$s = 1$	0

where \bar{x} and x_i are the average deposition rate and the growth rate of the i th location of the area, respectively, S_i and S are the area of the i th location and the area of the zones between a and b , respectively and C is the coefficient of variation.

3. Physical model

3.1. Geometry description

The simulation was carried out in an independently developed conceptual reactor, containing seven 6-inch wafers for GaN-MOCVD, as shown in figure 1. The carrier gas consists of a mixture of N_2 and H_2 . The group III source element, Ga, and the group V source, N, are uniformly sprayed into the reactor

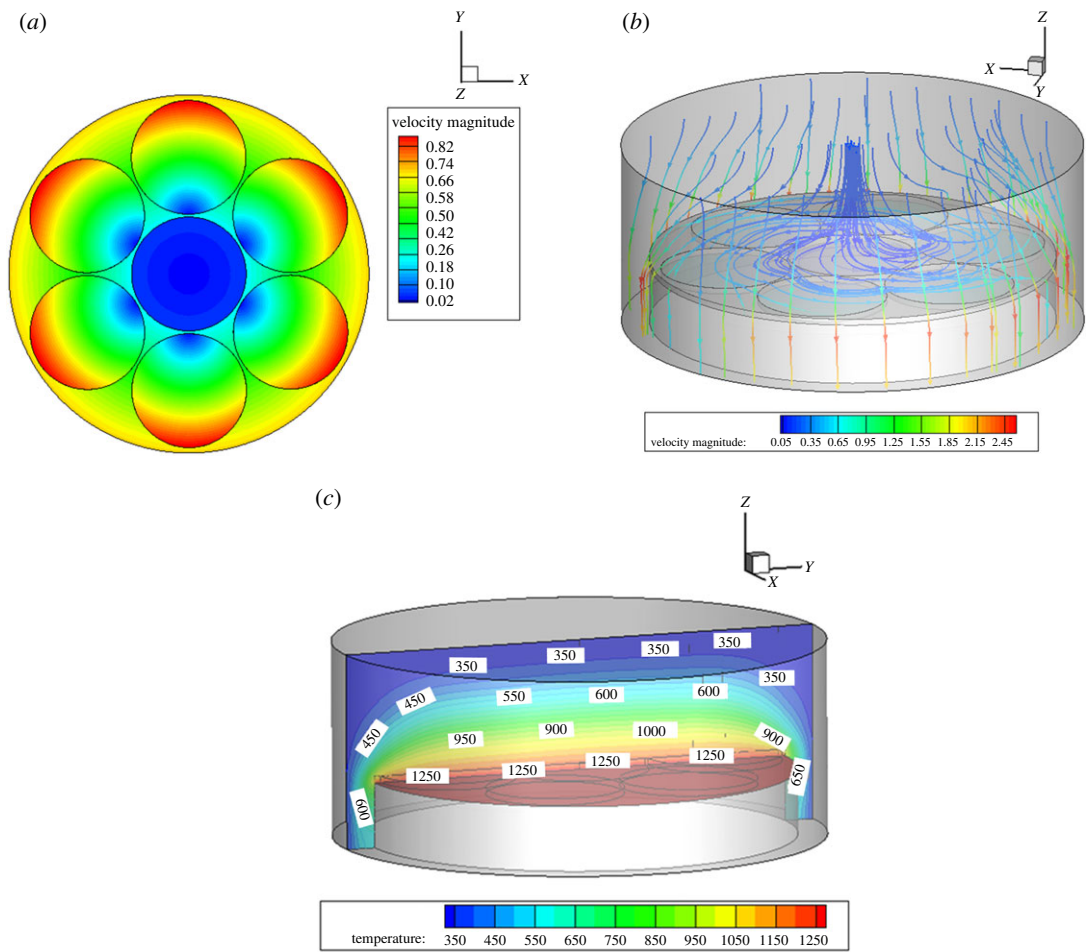


Figure 3. (a) Substrate rotation speed in different regions. (b) Velocity streamline diagram in MOCVD. (c) Temperature profile of reaction chamber.

Table 3. Simulation parameters.

susceptor temperature (K)	1273	gas inlet temperature (K)	300	A rotation speed (r.p.m.)	20
gas velocity (m s^{-1})	0.2	outer wall temperature (K)	300	B rotation speed (r.p.m.)	5
reactor pressure (torr)	12.5	mole percentage of NH_3 (%)	0.21	C rotation speed (r.p.m.)	20
				(relative to the B region)	
mole percentage of TMG (%)	0.00091	mole percentage of H_2 (%)	0.51		

through vertical pipes. After the gas mixture flows through the heated substrate, these two components chemically react to produce monomer molecules, which collide, condense, crystallize and grow into a molecular cloud of particles to eventually form a heterostructured thin film on the substrate surface. The molecular cloud that is not deposited on the substrate leaves the reactor with the unused reactants, by-products and carrier gas through the exhaust flow channel on the sidewall.

The turntable is rotated in three areas, with A being the rotation speed of the substrate, B the central wafer rotation speed and C the rotation speed of the surrounding six wafers, as labelled in figure 1a. In order to ensure uniform deposition rate, the substrate and the seven wafers rotate at different speeds. The deposition rate is affected by many factors, such as the gas inlet velocity, substrate rotation speed and pressure in the reactor. In addition, the substrate is large, which creates difficulties in achieving uniform film thickness. Therefore, 12 points are selected on the substrate to study the speed regularity in different regions of the turntable. Average deposition rate along the circles is adopted to measure the thin film thickness.

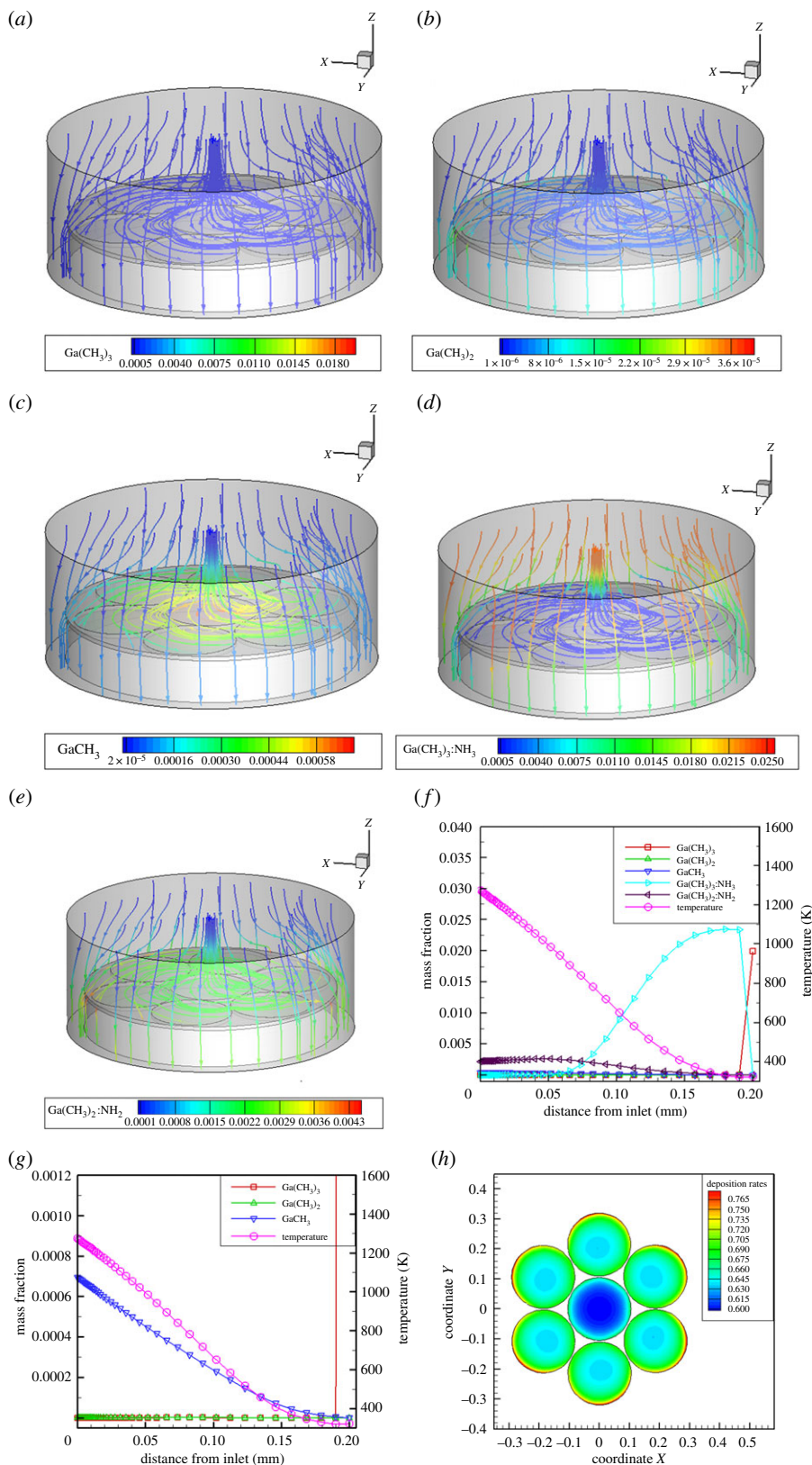


Figure 4. Mass fractions of Ga-containing species under reference conditions in MOCVD. (a) $\text{Ga}(\text{CH}_3)_3$, (b) $\text{Ga}(\text{CH}_3)_2$, (c) GaCH_3 , (d) $\text{Ga}(\text{CH}_3)_2:\text{NH}_3$, (e) $\text{Ga}(\text{CH}_3)_2:\text{NH}_2$. Mass fractions of Ga-containing species along the symmetry axis of MOCVD under reference conditions; (f) all species; (g) low-concentration species. (h) Film deposition rate.

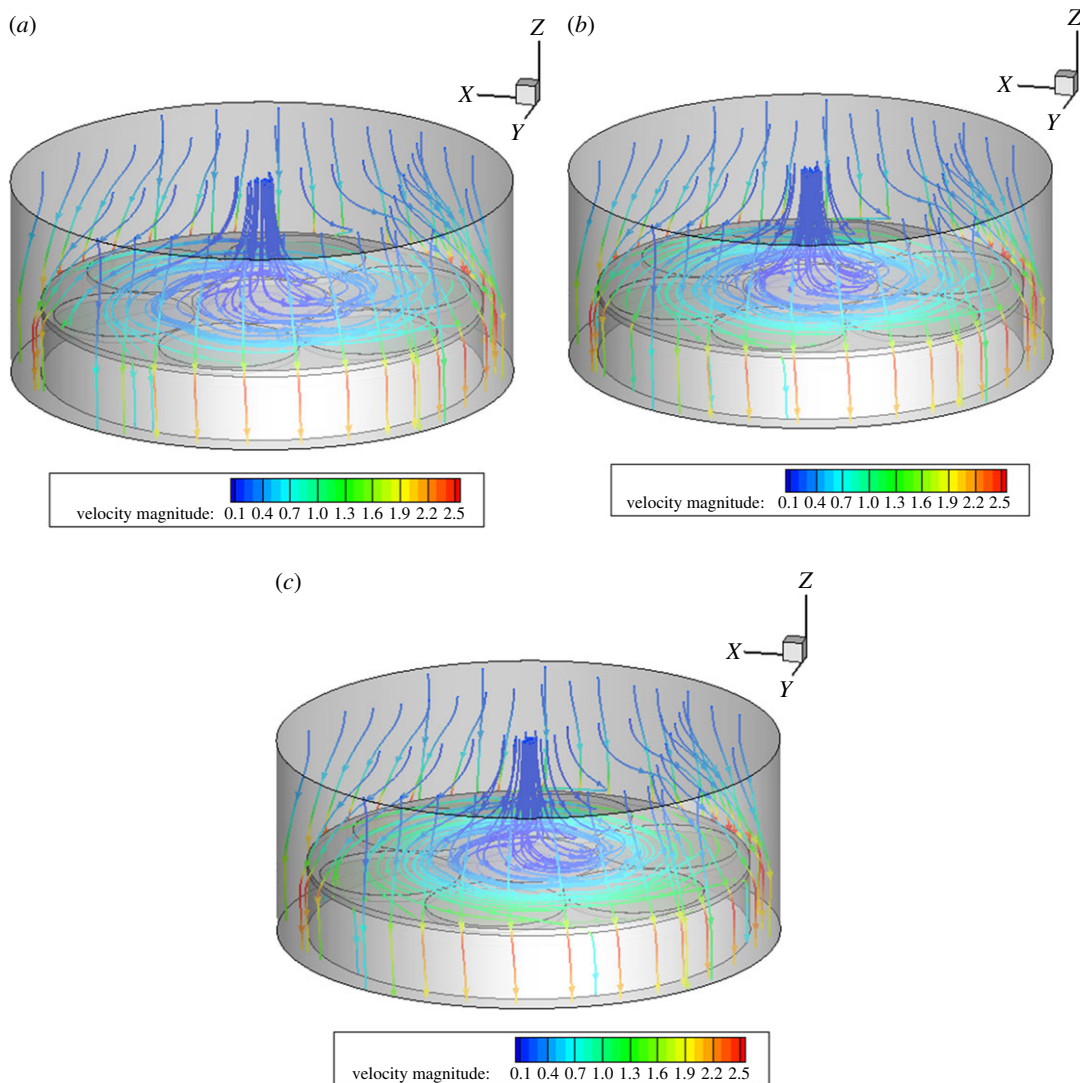


Figure 5. Velocity streamline diagram at different speeds in region A. (a) 30, (b) 40 and (c) 50 r.p.m.

3.2. Boundary conditions

As shown in figure 2, a hexahedral mesh and local refinement are used in areas where the flow rate and temperature gradient are large. We ensure numerical accuracy of the flow field in the reactor by maintaining the same mesh density in the intersection. Before we start the experiment, a grid sensitivity analysis is performed for the MOCVD reactor model to check its grid independency.

The uniformity of film thickness is not a dimensioned value, and it can be indicated by the coefficient of variation. Generally, the smaller the coefficient of variation, the smaller the degree of numerical dispersion, and the more uniform the film thickness.

The system was modelled using the Fluent (v. 14.0) fluid dynamics software. The convergence criteria were that the residual value of the energy is less than 10^{-6} , and the other variables are less than 10^{-4} .

The following boundary conditions were imposed:

- (1) The growth of the semiconductor material is a continuous transient-state process under the control of mass transmission.
- (2) The simulation parameters are provided in table 3 and the boundary conditions are set on the basis that the flow rate of the carrier gas, operating pressure, temperature and rotation speed of the substrate are changed within a certain range.
- (3) Laminar flow is adopted because the Reynolds number is less than 2300.

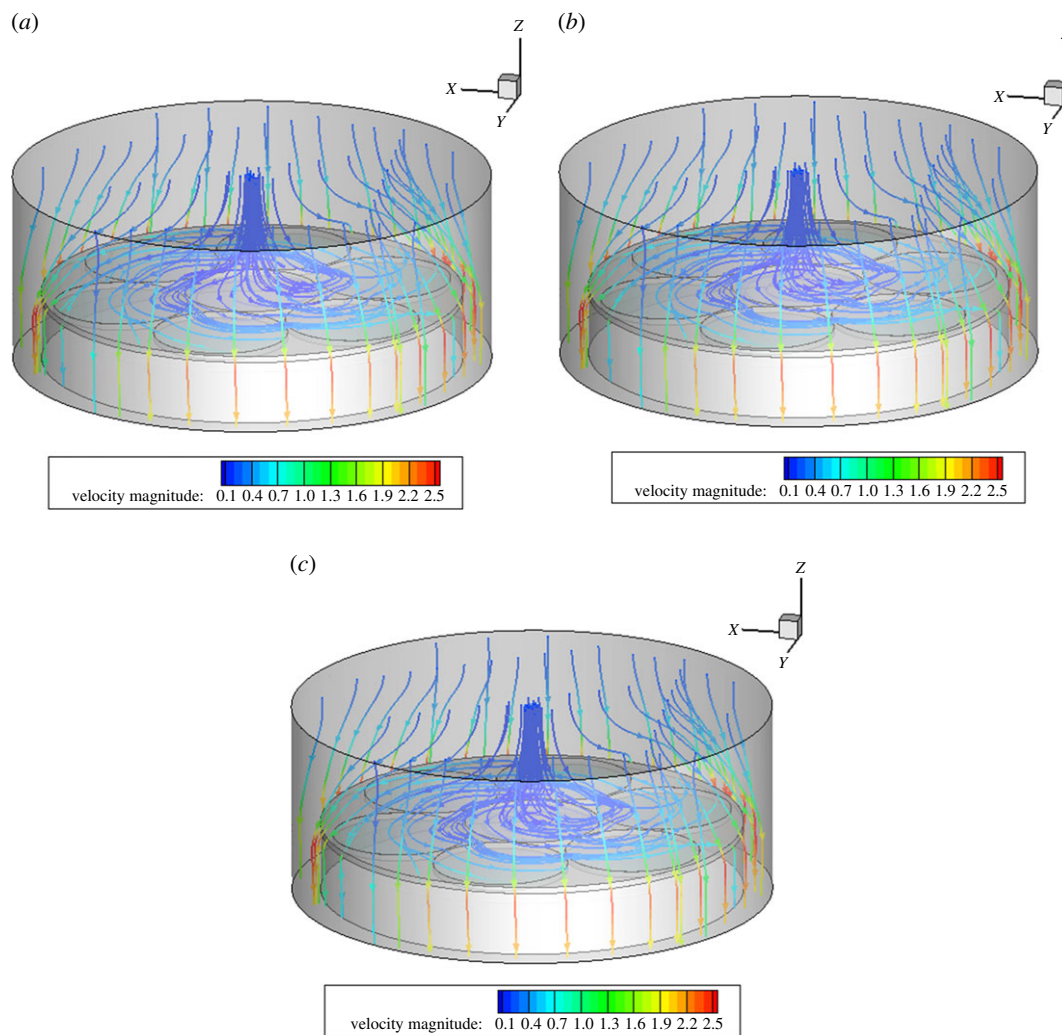


Figure 6. Velocity streamline diagram at different speeds in region B. (a) 10, (b) 15 and (c) 20 r.p.m.

- (4) The graphite plate has good thermal conductivity and the temperature difference within the susceptor is very small, considering that the temperature is constant.
- (5) A pressure-outlet boundary condition is adopted such that the given outlet static pressure is 0 Pa.

4. Results and discussion

4.1. Simulation results under the reference conditions

The results in figure 3 present the flow field, temperature field and deposition rate of the MOCVD reaction chamber under the conditions given in table 1. Figure 3*a* shows the velocity profiles of three regions at different rotation speeds. The flow velocity at the inlet, thermal buoyancy and the flow field of each turntable of the substrate are shown in figure 3*b*. It can also be seen that the inner ring of the entrance acts to encourage gas deposition over the substrate, and the outer ring acts to stabilize the flow field. Figure 3*c* shows the temperature contours in the reaction chamber. The temperature boundary layer, which has a large temperature gradient, is within 5 mm of the substrate surface. The temperature distribution outside the boundary layer is relatively uniform, in the range of 1100–1273 K, which is suitable for the growth and deposition of thin films.

Figure 4*a–e* is the mass fraction cloud chart distribution of each Ga component in the reaction chamber under the reference conditions. Figure 4*f,g* shows the mass fraction distribution of each component along

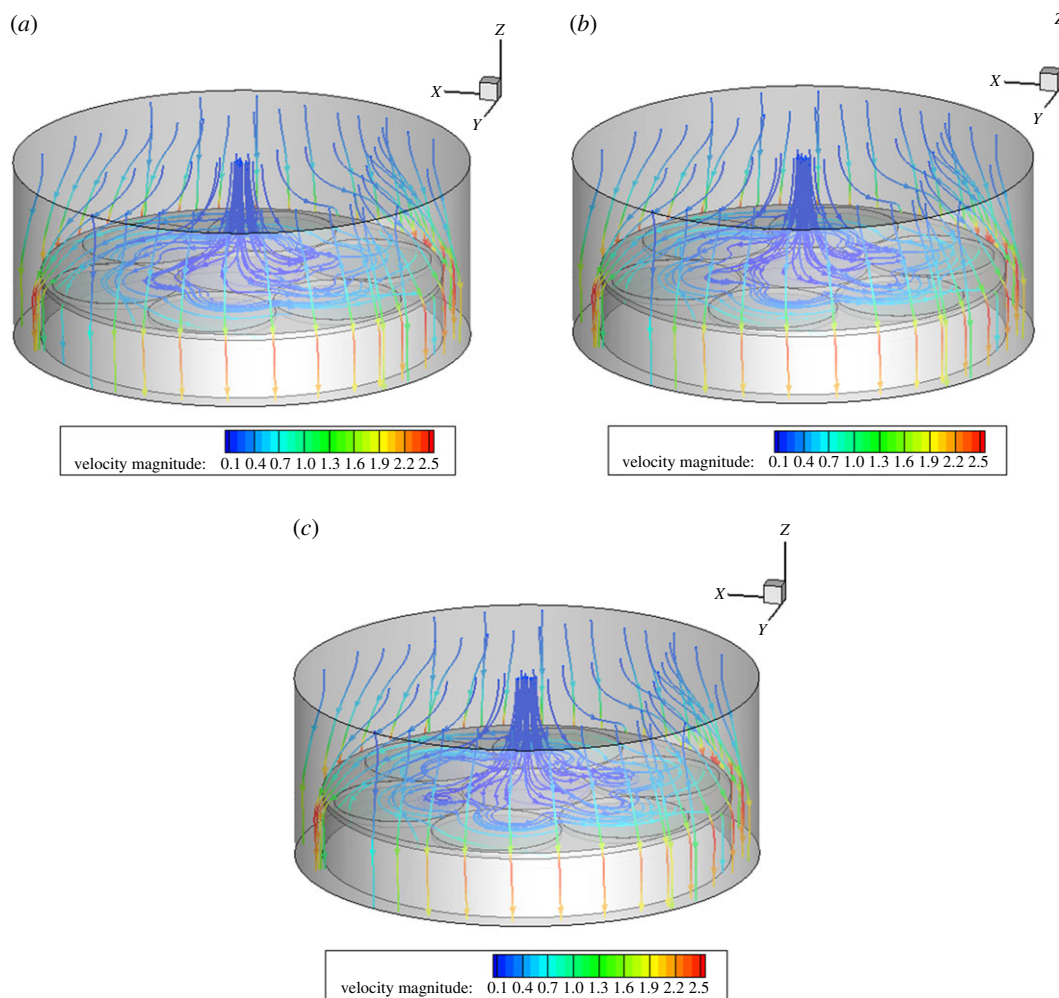


Figure 7. Velocity streamline diagram at different speeds in region C. (a) 30, (b) 40 and (c) 50 r.p.m.

the central axis of the reactor. Combined with the two diagram observations, it is known that in the upper part of the substrate, because reaction G3 does not need activation energy, $\text{Ga}(\text{CH}_3)_3$ and NH_3 will quickly form adducts (G3) in the reaction chamber. The adduct is filled in the range of distance entrance 1 mm. When the adduct is near the high-temperature boundary layer, $\text{Ga}(\text{CH}_3)_3:\text{NH}_3$ decomposes backward to generate $\text{Ga}(\text{CH}_3)_3$ and NH_3 (G4), and the maximum concentration is generated at a distance of 5 mm from the inlet, where the temperature is about 400 K. However, the undecomposed $\text{Ga}(\text{CH}_3)_3:\text{NH}_3$ is diffused to the high-temperature area and removed CH_4 to produce an amino group $\text{Ga}(\text{CH}_3)_2:\text{NH}_2$ (G5). The maximum concentration occurred at the distance entrance 12.5 mm, where the temperature is about 900 K. The amino compounds continue to deposit here to produce GaN films. At the same time, when the temperature rises to the activation energy barrier, which can be crossed over in reactions G1 and G2, $\text{Ga}(\text{CH}_3)_3$ will be further decomposed, and $\text{Ga}(\text{CH}_3)_2$ and GaCH_3 will be generated near the substrate. However, the $\text{Ga}(\text{CH}_3)_3$ concentration of the product of direct decomposition of GaCH_3 is at least two orders of magnitude lower than the product of its addition reaction, $\text{Ga}(\text{CH}_3)_2:\text{NH}_2$. The deposition rate of the substrate film is shown in figure 4*h*; however, it can be seen that the deposition rate is very uneven, with a film thickness variation coefficient of 5.94%. Therefore, we studied the speed of each region in order to obtain a more uniform deposition rate.

4.2. Influence of rotational speed on the flow field and temperature field

When other benchmark conditions are unchanged, and when the rotation speeds of region A are 30, 40 and 50 r.p.m., the rotation speeds of different bases have little influence on the flow field of the reaction chamber. In the intersection area of the turntables A and C, the streamline becomes more fluent with the

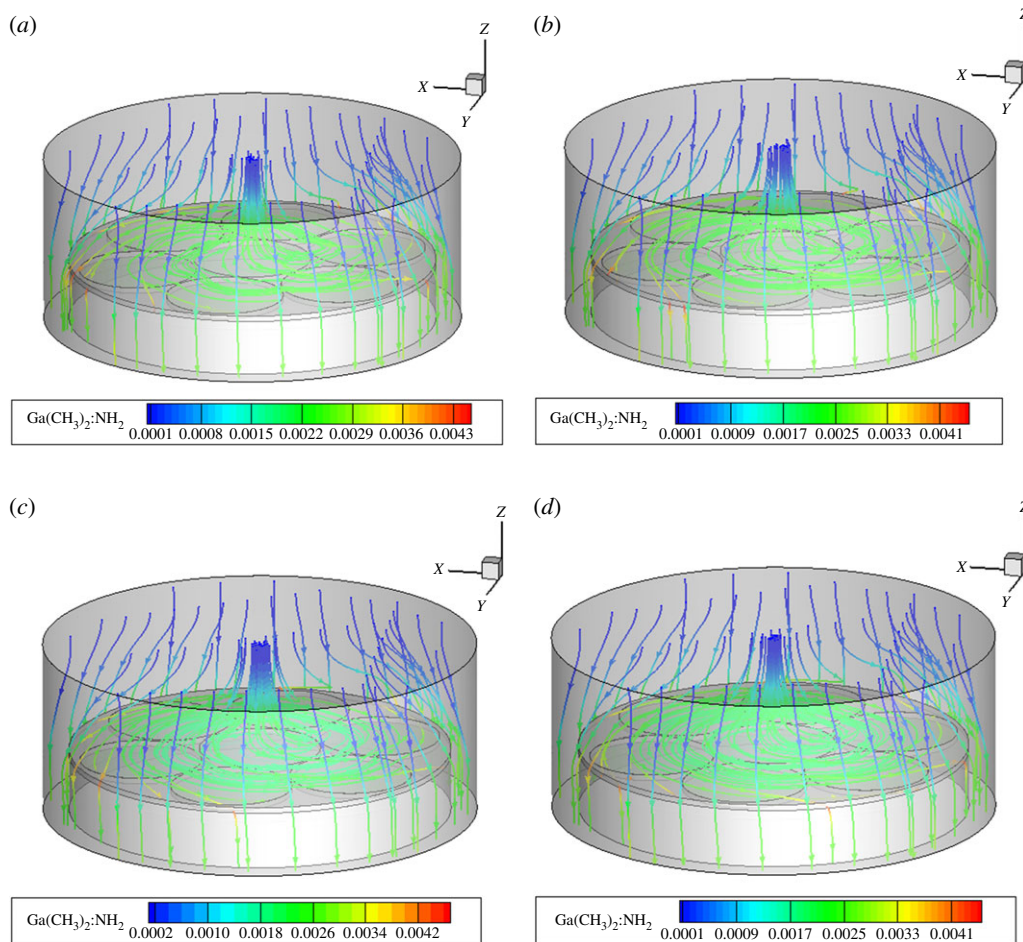


Figure 8. Mass fractions of $\text{Ga}(\text{CH}_3)_2\text{:NH}_2$ of MOCVD under the rotation conditions of region A. (a) 20, (b) 30, (c) 40 and (d) 50 r.p.m.

increase in the speed, and the flow-field distribution on the base still keeps more uniform and straight, as shown in figure 5.

When other benchmark conditions are unchanged, and when the rotation speeds of region B are 10, 15 and 20 r.p.m., the rotation speeds of different bases have little influence on the flow field in the reaction chamber. The distribution diagram of the flow field at the three speeds is basically similar, and the distribution of the flow field is even more uniform above the base, as shown in figure 6.

When other benchmark conditions are unchanged, and when the rotation speeds of region C are 30, 40 and 50 r.p.m., the rotation speeds of different bases have certain influence on the flow field of the reaction chamber. Three-speed flow-field distribution is slightly different in the intersection region of substrates A and C with the increase in the rotational speed fluctuations. With the increase of speed and cyclotron eddy above substrate C, it will have a certain impact on the film deposition. Above the base, a relatively uniform distribution flow is maintained, as shown in figure 7.

The different rotational speeds of the substrates of the three regions have little effect on the temperature field of the reaction chamber, which is basically consistent with that shown in figure 3c. (For further details, refer to electronic supplementary material, figures S1–S3.) Because the rotation speed does not increase significantly, it does not affect the temperature field in speed range.

4.3. Influence of rotational speed on species transport

Figures 8–10 show the mass fraction of the $\text{Ga}(\text{CH}_3)_2\text{:NH}_2$ components in MOCVD at the three regions at the speed of the region. The change in the substrate speed also does not change the relative size of the material concentration in the boundary layer, and changes only slightly under the influence of the speed. All the components of the three regions at different speeds are shown in the support file electronic supplementary material, figures S4–S15.

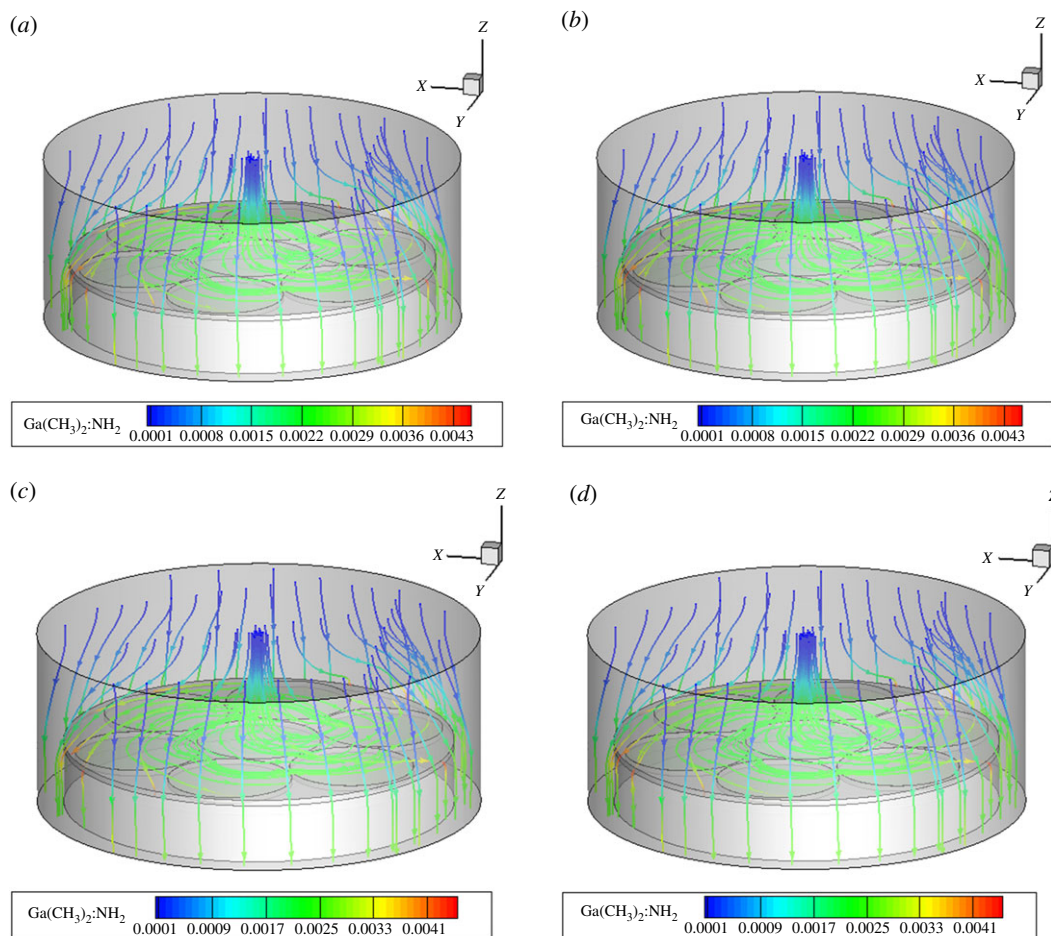


Figure 9. Mass fractions of $\text{Ga}(\text{CH}_3)_2:\text{NH}_2$ of MOCVD under the rotation conditions of region B. (a) 5, (b) 10, (c) 15 and (d) 20 r.p.m.

In the three regions and at different rotational speeds, the concentration distribution of substances in the concentration boundary layer is $\text{Ga}(\text{CH}_3)_2:\text{NH}_2$, GaCH_3 and $\text{Ga}(\text{CH}_3)_2$, and $\text{Ga}(\text{CH}_3)_3$ and $\text{Ga}(\text{CH}_3)_3:\text{NH}_3$ disappear in the cavity. That is, the speed of changing the substrates of different regions does not change the rule that the $\text{Ga}(\text{CH}_3)_3$ and the NH_3 plus-pyrolysis paths dominate. The main growth precursors of the film growth are still $\text{Ga}(\text{CH}_3)_2:\text{NH}_2$ and GaCH_3 .

In summary, the characteristics of planetary MOCVD involve material deposition at low rotational speeds. Therefore, changing the substrate speed in a relatively low range will not change the overall temperature field, flow field and component distribution. It will also not affect the dominance of addition and pyrolysis paths in MOCVD. It only affects the concentration change of the Ga gas component near the substrate rotation region, which further affects the change in the film deposition rate.

4.4. Influence of rotational speed on deposition rate

In the case of other conditions being unchanged, the deposition rate changed as the rotation speeds increase, as shown in figure 11. Figure 11*a,b* shows the deposition rate dependence on the rotation speed of region A. As the speed increases, the growth rate increases slightly, while the growth uniformity becomes slightly variable. This shows that the effect of substrate rotation speed on deposition rate and composition distribution is very small. Figure 11*c,d* shows the deposition rate dependence on the rotation speed of region B. The surrounding wafers are symmetrically distributed and rotate at the same speed, and the upper gas flow includes the central wafer to drive the uniform spread of the air distribution. As the speed increases, the growth rate and the growth uniformity again increase by a small amount. Figure 11*e,f* shows the deposition rate dependence on the rotation speed of region C. Rotation of the central wafer causes central cavity flow; with increasing speed, both the growth rate and the growth uniformity increase first, and then decrease. The central cavity flow not only causes the gas flow to

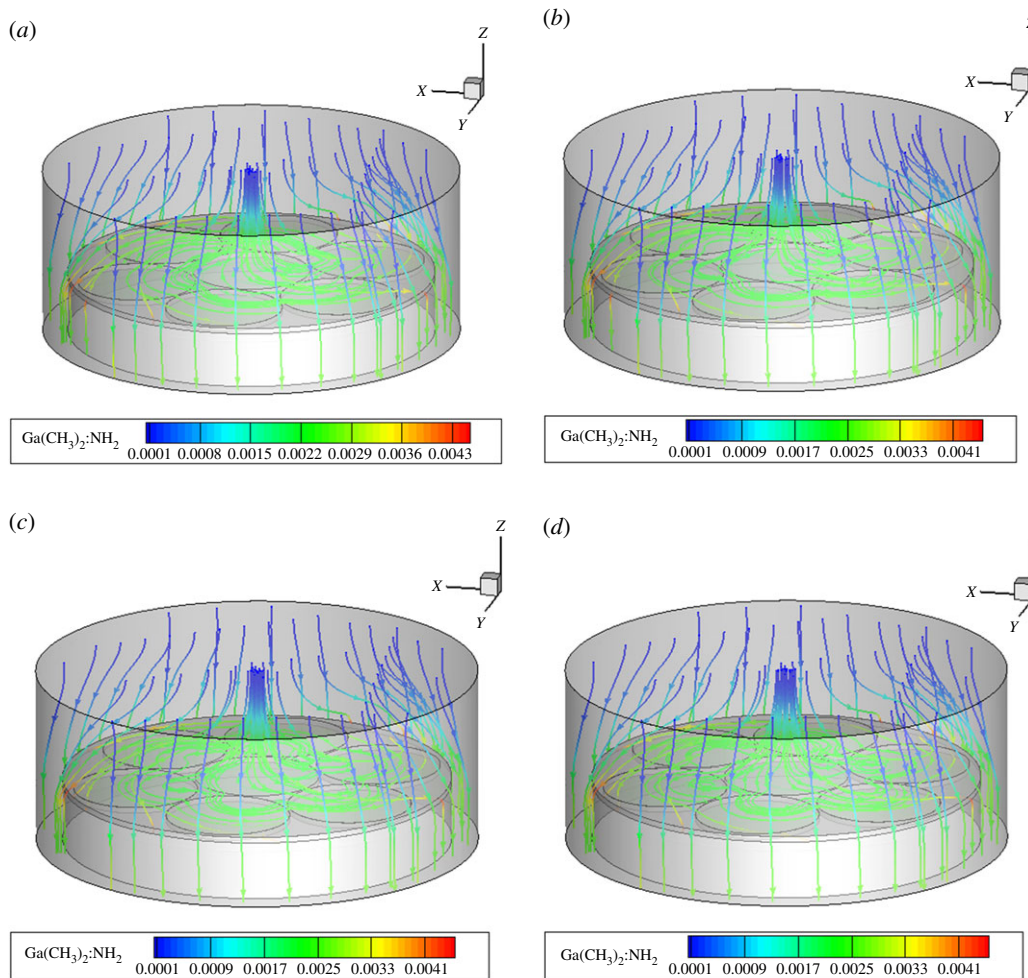


Figure 10. Mass fractions of $\text{Ga}(\text{CH}_3)_2:\text{NH}_2$ of MOCVD under the rotation conditions of region C. (a) 20, (b) 30, (c) 40 and (d) 50 r.p.m.

spread around the substrate but also promotes an overall uniform airflow. It shows that the influence of central wafer rotation speed on the deposition rate distribution is relatively large. Figure 11 shows that in the intersection of the inner ring and the outer circle, due to the mismatch of the speed and the flow field, the deposition rate of the connecting parts in the two regions is significantly changed.

5. MOCVD process parameters optimization

5.1. The optimization goal and optimization scheme

Rotation speeds of the substrate, central wafer and surrounding wafers are $X = \{x_1, x_2, x_3\}$, and the average deposition rates of 12 circles are $Y = \{y_1, y_2, y_3, y_4, y_5, y_6, y_7, y_8, y_9, y_{10}, y_{11}, y_{12}\}$.

We propose that the problem of film thickness uniformity control is converted to the question: how to adjust the rotation speeds X to minimize the coefficient of variation of film uniformity.

$$\text{Min } C(Y): Y = f(X) \quad 5 \leq x_1 \leq 20; \quad 20 \leq x_2 \leq 50; \quad 20 \leq x_3 \leq 50. \quad (5.1)$$

where, x_i is the different zone speed, $f(X)$ is the function between the inlet velocity and the average deposition rate, and $C(Y)$ is the function of film thickness variation coefficient.

In order to obtain the most uniform film thickness, the variation coefficient of the 12 average deposition rates must be minimized. If the other conditions remain unchanged, the optimal result is obtained by adjusting the values of A, B and C, as shown in table 4.

Numerical simulation takes a lot of time; thus, complete simulation using all the possible range of values of rotation speed will be a very large and time-consuming project. Therefore, in this study an

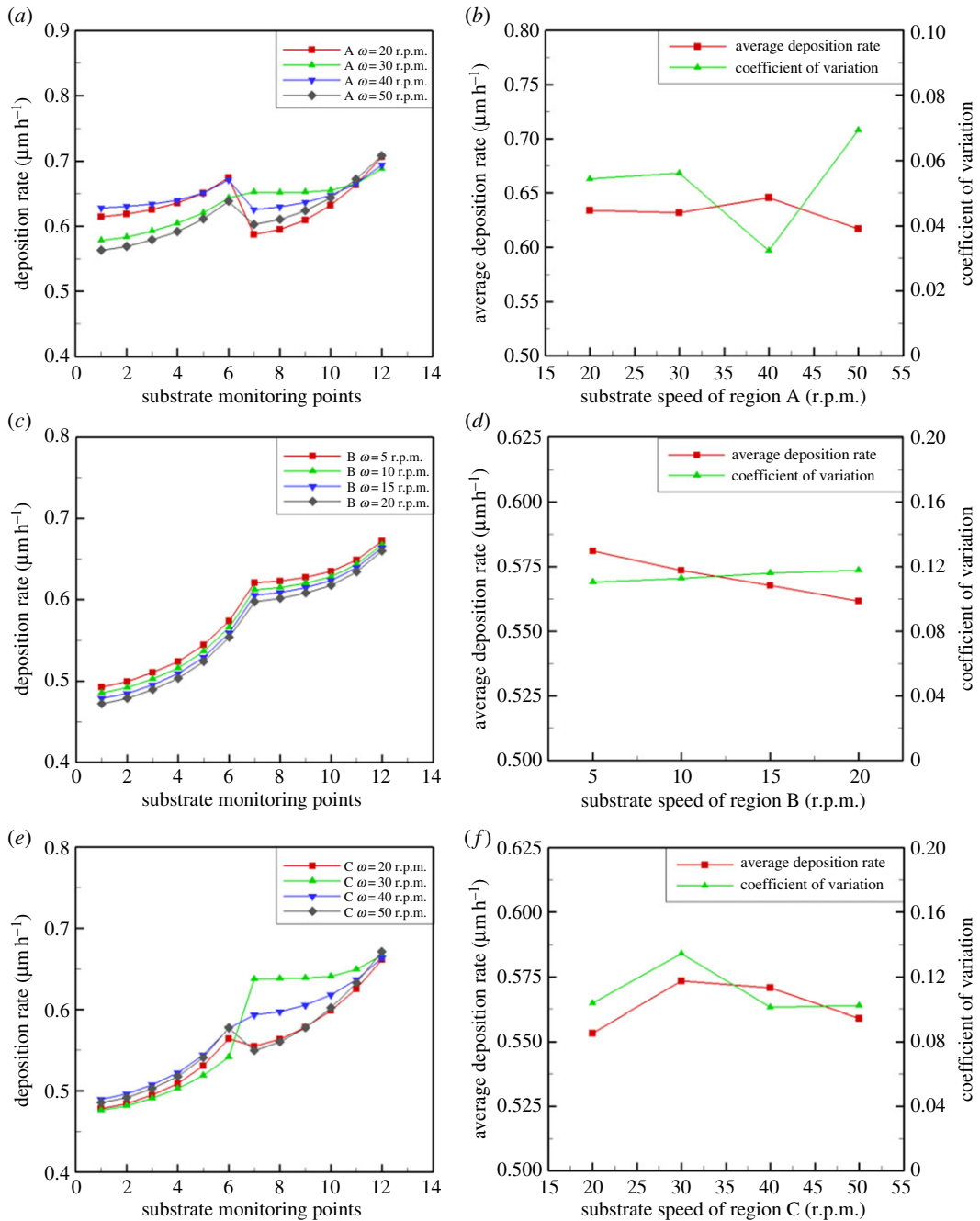


Figure 11. Effect of region A rotation speed on (a) deposition rate and (b) coefficient of variation. Effect of region B rotation speed on (c) deposition rate and (d) coefficient of variation. Effect of region C rotation speed on (e) deposition rate and (f) coefficient of variation.

Table 4. MOCVD process parameters.

variables (r.p.m.)	A	B	C
lower bound (r.p.m.)	20	5	20
upper bound (r.p.m.)	50	20	50
output	12 average deposition rates		

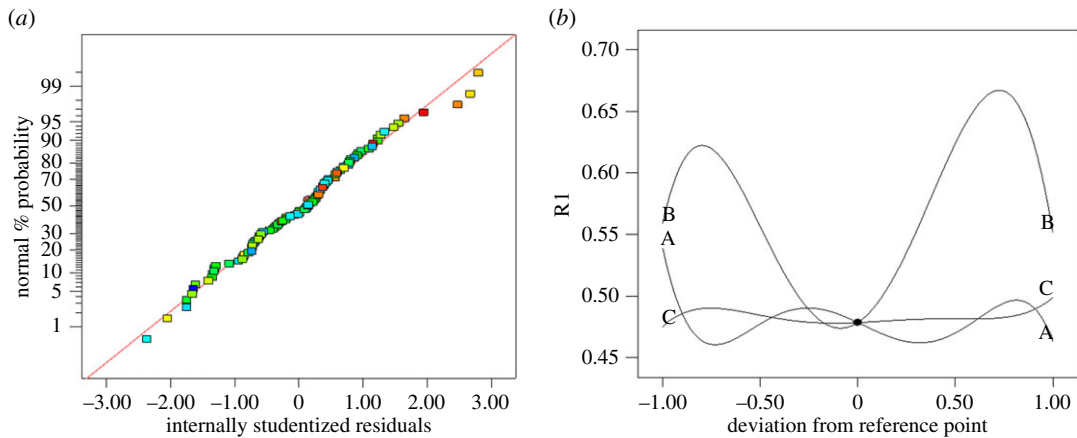


Figure 12. (a) Normal probability plot of residuals. (b) Influence of speed in different regions.

RSM method was used. One hundred sets of data were simulated by adjusting the values of A, B and C, and then these 100 sets of inputs (A, B and C) and outputs (12 deposition rates) were used to construct the input and output mapping relationship. Then 10 sets of new data were randomly selected to verify the accuracy of the model. Finally, a genetic algorithm was used to optimize the response surface model to find the most uniform (minimum coefficient of variation) result.

5.2. Construction and analysis of RSM model

The model has 12 deposition rate results; however, we can select just one of the results of the analysis due to the other results being similar. Figure 12a shows the normal probability plot of residuals, in which most of the points are in the normal distribution, and the fitting results of the model are very good. Figure 12b shows the effect of a single variable on the outcome: B value is the most influential, followed by A, with C having the least impact.

The substrate rotation speed, A, has a small numerical change range, and is acting on the gas flow in the whole reactor, so that the change is relatively stable. The rotation speed of the central wafer, B, causes a vortex generated by rotation to spread throughout the reaction chamber, so that the local vortex drives the airflow distribution in the whole chamber to drive the reactant diffusion around, and thus has the greatest impact on deposition rate. The rotation speed, C, of the six circularly distributed wafers, and the induced vortices are symmetrical, resulting in the least impact. Thus, the influence of different rotating speeds on the flow field leads to the change of deposition rate of substrate film.

Figure 13 shows the three-dimensional response surface model diagram, which illustrates the effect of the interaction of two parameters on the result. It not only shows the single factor effect, which is included in figure 12b, but also shows the interaction of two factors of A, B and C. From a single factor A surface alone, as the rotation speed increases, the fluctuation trends of A and figure 12b are in agreement; the same is true for factors B and C. The surface showing the A and C coupled effect is not stable, leading to the difference in deposition rate. However, the surfaces of B and C are coupled, and the A and B coupled effect is relatively stable.

5.3. Predication performance of RSM model and optimization result

Eight sets of new data were randomly selected, as shown in the electronic supplementary material. The RSM-predicted results were compared with the CFD simulation results and the average deposition rate error is no more than 5%. Therefore, the RSM-predicted and simulated values are consistent in both the numerical values and the changing trends, and for the subsequent optimization of the coefficient of variation, it is highly dependent on the accuracy of trend. Therefore, the RSM model can be used as the corresponding model for the input and output of the MOCVD reactor, which is used for the following optimization process.

Based on the corresponding relation of the input and output, the genetic algorithm is used to find the parameter value of the minimum coefficient of variation of the 12 deposition rates. The optimization results are shown in figure 14. The optimal rotation speeds are A = 40 r.p.m., B = 18 r.p.m. and C = 24 r.p.m., which provide a variation coefficient of 1.87%.

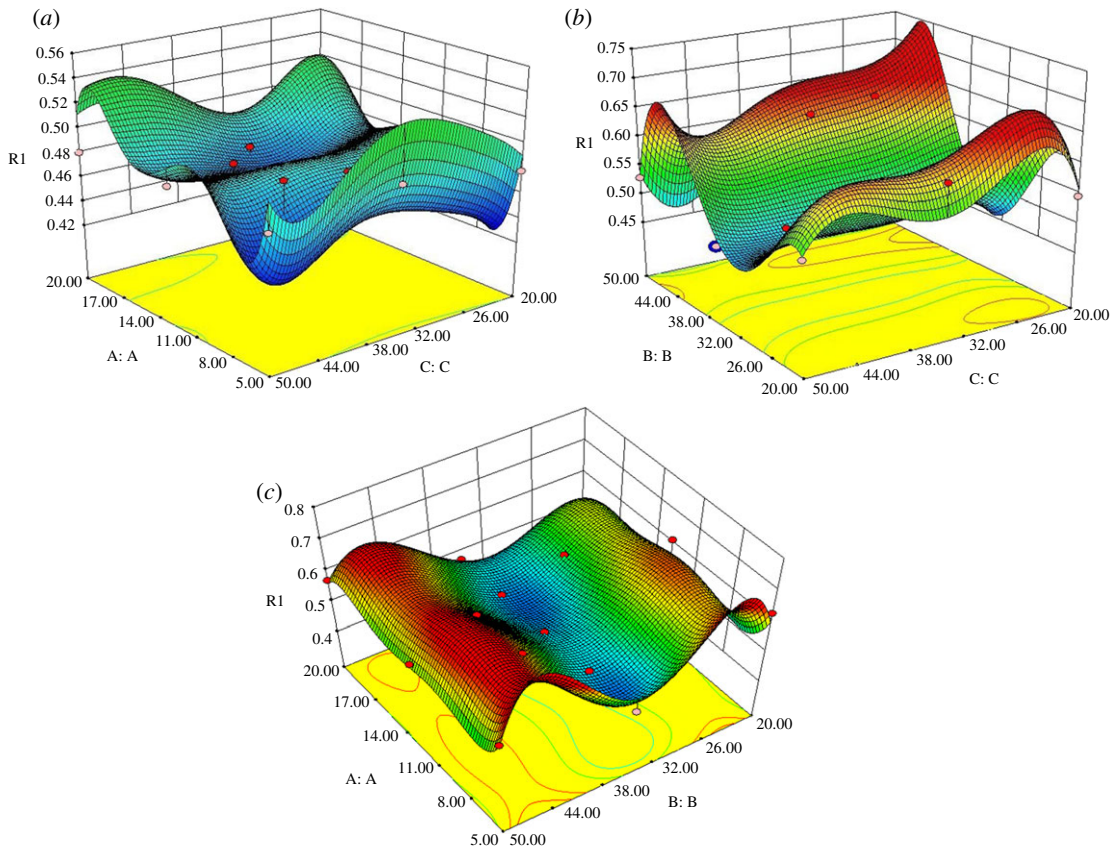


Figure 13. Three-dimensional RSM diagram of the influence of different regions on substrate deposition rate. (a) A and C coupled effect. (b) B and C coupled effect. (c) A and B coupled effect.

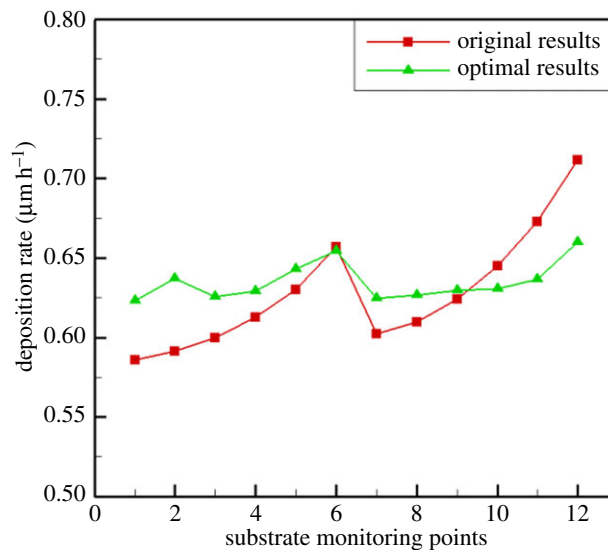


Figure 14. Deposition rate distribution of the optimized substrate.

6. Conclusion

In this study, the MOCVD planetary and wafer rotation speeds were optimized for uniform film thickness, by both numerical simulation and using an RSM model. The important conclusions from this study are as follows.

- (1) When the inlet flow rate, turntable temperature and internal pressure are stable, the influence of different speed regions on the temperature field is not obvious, but there is a certain disturbance

in the speed and species, further affecting the deposition rate. Especially with the increase in the speed of region C, the disturbance is more obvious.

- (2) The accuracy of the RSM model is high, such that the predicted value and simulation value can be used to map the relationship between inputs and outputs, and it can be used to optimize the process parameters. The optimum rotation speed of different regions is obtained by using the optimized model, which provides a theoretical basis for obtaining the best film deposition rate. The coefficient of variation of film thickness across the entire substrate is reduced from 5.00 to 1.87%.
- (3) A model with a large number of grids is used to construct the RSM model, which can investigate the influence of each process parameter on the result, significantly reducing simulation time and cost.

Data accessibility. Data accompanying this paper can be found at Dryad (<http://dx.doi.org/10.5061/dryad.63821>) [36].
Authors' contributions. J.L. carried out the CFD work, and participated in data analysis; Z.-y.F. carried out research on parameters optimization; Y.-f.X. carried out sequence alignments, and participated in the design of the study and drafted the manuscript; J.W. carried out the statistical analyses; X.-j.M. collected field data; B.-f.F. conceived the study, and designed the study; G.W. coordinated the study and helped draft the manuscript.

Competing interests. We declare that we have no competing interests.

Funding. We acknowledge the financial support from Natural Funds of Guangdong Province (grant no. 2015A030311050, all the authors).

Acknowledgements. We appreciate the equipment support from the National Supercomputing Center (NSCC) in Guangzhou.

References

1. Stringfellow GB. 1999 *Organometallic vapor-phase epitaxy: theory and practice*, p. 6. New York, NY: Academic Press.
2. Sze SM. 2003 *Semiconductor devices: physics and technology*, p. 26, 2nd edn. Hsinchu, Taiwan: NCTU Press. (in Chinese)
3. Navamathavan R, Ra YH, Song KY, Kim DW, Lee CR. 2011 Different growth behaviors of GaN nanowires grown with Au catalyst and Au + Ga solid solution nano-droplets on Si(111) substrates by using MOCVD. *Curr. Appl. Phys.* **11**, 77–81. (doi:10.1016/j.cap.2010.06.022)
4. Wang Y, Xu Y, Yang Y, Gao X, Zhu B, Cai W, Yuan J, Zhang R, Zhu H. 2016 Simultaneous light emission and detection of InGaN/GaN multiple quantum well diodes for in-plane visible light communication on a chip. *Optics Commun.* **387**, 440–445. (doi:10.1016/j.optcom.2016.10.070)
5. Lin S, Li X, Pan H, Chen H, Li X, Li Y, Zhou J. 2016 Numerical analysis of In_xGa_{1-x}N/SnS and Al_xGa_{1-x}N/SnS heterojunction solar cells. *Energy Convers. Manage.* **119**, 361–367. (doi:10.1016/j.enconman.2016.04.059)
6. Lu M, Zhang GG, Fu K, Yu GH, Su D, Hu JF. 2011 Gallium nitride Schottky betavoltaic nuclear batteries. *Energy Convers. Manage.* **52**, 1955–1958. (doi:10.1016/j.enconman.2010.10.048)
7. Sytniewski ŁJ, Lapkin AA, Stepanov S, Wang WN. 2008 CFD optimisation of up-flow vertical HVPE reactor for GaN growth. *J. Cryst. Growth* **310**, 3358–3365. (doi:10.1016/j.jcrysgro.2008.04.017)
8. Akasaki I, Amano H. 1995 Crystal growth of column III nitrides and their applications to short wavelength light emitters. *J. Cryst. Growth* **146**, 455–461. (doi:10.1016/0022-0248(94)00501-X)
9. Leathersich J, Arkun E, Clark A, Suvarna P, Marini J, Dargis R, Shahedipour-Sandvik F. 2014 Deposition of GaN films on crystalline rare earth oxides by MOCVD. *J. Cryst. Growth* **399**, 49–53. (doi:10.1016/j.jcrysgro.2014.04.015)
10. Cheng Y, Zong H, Wu J, Liu P, Han T, Yu T, Hu X, Zhang G. 2016 Exceptionally long GaN sub-micrometer rods grown by HVPE on a MOCVD-GaN rod template. *J. Alloys Compd.* **688**, 967–971. (doi:10.1016/j.jallcom.2016.07.115)
11. Kushvaha SS, Ramesh C, Tyagi P, Shukla AK, Yadav BS, Dilawar N, Maurya KK, Kumar MS. 2017 Quantum confinement effect in low temperature grown homo-epitaxial GaN nanowall network by laser assisted molecular beam epitaxy. *J. Alloys Compd.* **703**, 466–476. (doi:10.1016/j.jallcom.2017.02.006)
12. Wu B, Ma R, Zhang H. 2003 Epitaxy growth kinetics of GaN films. *J. Cryst. Growth* **250**, 14–21. (doi:10.1016/S0022-0248(02)02208-X)
13. Mucciato R, Lovergine N. 2000 Detailed thermal boundary conditions in the 3D fluid-dynamic modelling of horizontal MOVPE reactors. *J. Cryst. Growth* **221**, 758–764. (doi:10.1016/S0022-0248(00)00812-5)
14. Xenidou TC, Boudouvis AG, Markatos NC, Samélor D, Senocq F, Prudhomme N, Vahlas C. 2007 An experimental and computational analysis of a MOCVD process for the growth of Al films using DMEAA. *Surf. Coat. Technol.* **201**, 8868–8872. (doi:10.1016/j.surfcoat.2007.04.080)
15. Dam CEC, Hageman PR, Larsen PK. 2005 Carrier gas and position effects on GaN growth in a horizontal HVPE reactor: an experimental and numerical study. *J. Cryst. Growth* **285**, 31–40. (doi:10.1016/j.jcrysgro.2005.08.006)
16. Maejima K, Fujita S. 2006 Chemical vapor reactions of ZnO growth by metal-organic vapor phase epitaxy. *J. Cryst. Growth* **293**, 305–310. (doi:10.1016/j.jcrysgro.2006.04.117)
17. Dimitrios I, Kremer AM, McKenna DR, Jensen KF. 1987 Complex flow phenomena in vertical MOCVD reactors: Effects on deposition uniformity and interface abruptness. *J. Cryst. Growth* **85**, 154–164. (doi:10.1016/0022-0248(87)90217-X)
18. Kuo WS, Wang CY, Tuh JL, Lin TF. 2005 Delayed onset of return flow by substrate inclination in model horizontal longitudinal MOCVD processes. *J. Cryst. Growth* **274**, 265–280. (doi:10.1016/j.jcrysgro.2004.09.097)
19. Fotiadis DI, Jensen KF. 1990 Thermophoresis of solid particles in horizontal chemical vapor deposition reactors. *J. Cryst. Growth* **102**, 743–761. (doi:10.1016/0022-0248(90)90838-C)
20. Theodoropoulos C, Mountziaris TJ, Moffat HK, Han J. 2000 Design of gas inlets for the growth of gallium nitride by metalorganic vapor phase epitaxy. *J. Cryst. Growth* **217**, 65–81. (doi:10.1016/S0022-0248(00)00402-4)
21. Parikh RP, Adomaitis RA. 2006 An overview of gallium nitride growth chemistry and its effect on reactor design: application to a planetary radial-flow CVD system. *J. Cryst. Growth* **286**, 259–278. (doi:10.1016/j.jcrysgro.2005.09.050)
22. Mitrovic B, Gurary A, Kadinski L. 2006 On the flow stability in vertical rotating disc MOCVD reactors under a wide range of process parameters. *J. Cryst. Growth* **287**, 656–663. (doi:10.1016/j.jcrysgro.2005.10.131)
23. Endres D, Mazumder S. 2010 Numerical investigation of pulsed chemical vapor deposition of aluminum nitride to reduce particle formation. *J. Cryst. Growth* **335**, 42–50. (doi:10.1016/j.jcrysgro.2011.08.041)
24. Bao Q, Zhu T, Zhou N, Guo S, Luo J, Zhao C. 2015 Effect of hydrogen carrier gas on AlN and AlGaN growth in AMEC Prismo D-Blue®; MOCVD platform. *J. Cryst. Growth* **419**, 52–56. (doi:10.1016/j.jcrysgro.2015.02.084)
25. Gkinis PA, Aviziotis IG, Koronaki ED, Gakis GP, Boudouvis AG. 2017 The effects of flow multiplicity on GaN deposition in a rotating disk CVD reactor.

- J. Cryst. Growth* **458**, 140–148. (doi:10.1016/j.jcrysgro.2016.10.065)
26. Lin CH, Cheng WT, Lee JH. 2009 Effect of embedding a porous medium on the deposition rate in a vertical rotating MOCVD reactor based on CFD modeling. *Int. Commun. Heat Mass Transf.* **36**, 680–685. (doi:10.1016/j.icheatmasstransfer.2009.03.019)
 27. Lan WC, Tsai CD, Lan CW. 2009 The effects of shower head orientation and substrate position on the uniformity of GaN growth in a HVPE reactor. *J. Taiwan Inst. Chem. Eng.* **40**, 475–478. (doi:10.1016/j.jtice.2008.12.008)
 28. Chuang YC, Chen CT. 2014 Mathematical modeling and optimal design of an MOCVD reactor for GaAs film growth. *J. Taiwan Inst. Chem. Eng.* **45**, 254–267. (doi:10.1016/j.jtice.2013.05.022)
 29. Han XF, Hur MJ, Lee JH, Lee YJ, Oh CS, Yi KW. 2014 Numerical simulation of the gallium nitride thin film layer grown on 6-inch wafer by commercial multi-wafer hydride vapor phase epitaxy. *J. Cryst. Growth* **406**, 53–58. (doi:10.1016/j.jcrysgro.2014.08.018)
 30. Tseng CF, Tsai TY, Huang YH, Lee MT, Horng RH. 2015 Transport phenomena and the effects of reactor geometry for epitaxial GaN growth in a vertical MOCVD reactor. *J. Cryst. Growth* **432**, 54–63. (doi:10.1016/j.jcrysgro.2015.09.003)
 31. Zhang Z, Fang H, Yao Q, Yan H, Gan Z. 2016 Species transport and chemical reaction in a MOCVD reactor and their influence on the GaN growth uniformity. *J. Cryst. Growth* **454**, 87–95. (doi:10.1016/j.jcrysgro.2016.09.010)
 32. Yu Y, Sun D, Wu K, Xu Y, Chen H, Zhang X, Qiu L. 2011 CFD study on mean flow engine for wind power exploitation. *Energy Convers. Manage.* **52**, 2355–2359. (doi:10.1016/j.enconman.2010.12.046)
 33. Al R. 2013 CFD simulation of air to air enthalpy heat exchanger. *Energy Convers. Manage.* **74**, 377–385. (doi:10.1016/j.enconman.2013.05.038)
 34. Alfarawi S, Al-Dadah R, Mahmoud S. 2016 Influence of phase angle and dead volume on gamma-type Stirling engine power using CFD simulation. *Energy Convers. Manage.* **124**, 130–140. (doi:10.1016/j.enconman.2016.07.016)
 35. Everitt BS. 2010 *The Cambridge dictionary of statistics[M]// The Cambridge dictionary of statistics in the medical sciences*, pp. 387–388. Cambridge, UK: Cambridge University Press.
 36. Li J, Fei Z, Xu Y, Wang J, Fan B, Ma X, Fan B, Wang G. 2018 Data from: Study on the optimization of the deposition rate of planetary GaN-MOCVD films based on CFD simulation and the corresponding surface model. Dryad Digital Repository. (doi:10.5061/dryad.63821)